IRSTI 27.35.29 https://doi.org/10.26577/ijmph.2024v15i2b7

Suman Sharma*, Shalini Jain

Department of Mathematics, University of Rajasthan, Jaipur-302004, India
*e-mail: s9549170542@gmail.com
(*Received 17 January 2024; revised 28 October 2024; accepted 23 November 2024)*

Convective heat transfer flow of MHD hybrid nanofluid over a stretching sheet with velocity and thermal slip

Abstract. In this study, we have investigated the convective heat transfer of a hybrid nanofluid with magnetohydrodynamic (MHD) properties over a permeable stretching sheet. The analysis takes into account the effects of velocity and thermal slip, and the hybrid nanofluid consists of two distinct nanoparticles–titanium dioxide *(TiO_2)* and silver *(Ag)*–dispersed in water *(H_2O)* as the base fluid. The use of *Ag* and *TiO_2* nano-composites is particularly significant in nano-biotechnology, especially in nano-medicine and cancer cell therapy, owing to their remarkable photocatalytic performances in handling pharmaceutical compounds and pollutants. The primary aim of this research is to explore how the behaviour of the MHD hybrid nanofluid over a permeable stretching surface is influenced by velocity and thermal slip conditions. By employing appropriate similarity transformations, the governing partial differential equations (PDEs) are transformed into dimensionless nonlinear ordinary differential equations (ODEs), which are then analytically solved using the Keller-box finite difference method. The results indicate that the velocity profile decreases with an increase in velocity slip, while the temperature and concentration fields decrease with thermal slip. The study further analyzes the significant impact of various parameters, including velocity and thermal slip parameter, porosity parameter, magnetic parameter, Prandtl number, and Eckert number, on the velocity, temperature, and concentration profiles. These findings are presented in graphical and tabular form, showing excellent agreement with previous literature.
Key words: Heat transfer, hybrid nanofluid, velocity slip, thermal slip, porous medium.

1. Introduction

High thermal conductivity is required for evolution of energy-efficient heat transfer. Initially, micro sized particles added to the base fluid by Maxwell. Choi introduced the term nanofluid, a fluid in which nanoparticles made of metals, carbides and oxide suspended in common fluids such as water, ethanol and ethylene glycol. These nanoparticles improve fluid properties such as thermal conductivity and specific heat etc. Nanofluid gained attention in many fields such as energy, industry, health with many applications as electronic cooling, automobile and heat exchangers. However, the applications of mono type nanofluid are limited. Single component nanofluid with metallic nanoparticles such as *Ag*, *Cu*, and *Al* has very high thermal conductivity, but they are unstable due to high reactivity. While the non-metallic nanoparticles as *CuO*, *MgO*, *Al_2O_3* have more stability but low conductivity. Now days, the researchers oriented their study towards hybrid nanofluid, an advanced kind of nanofluid prepared by suspending (i) two or more different type of nanoparticles in host fluid (ii) composite nanoparticles in regular single-phase liquid. In the last few years, the hybrid nanofluid gained abundant attention by researchers due to its energy storage applications such as heat exchanger in solar collectors, nuclear reactor cooling, photo electric devices, drug reduction, lubrication, optical fibre coating, cooling of electronic devices, coolant in machines, welding etc. Abu-Nada [1] investigated heat transfer enhancement in *CuO*-water nanofluid with the effect of thermal conductivity. Hejazian and Moravoji [2] analysed heat transfer for *TiO_2* nanofluid in a tube. Ramya et. al. [3] analysed viscous flow of nanofluid past a stretching sheet escorted by velocity and thermal slip.

Acharya et al. [4] compared the effect of variable thickness, magnetic field and variable temperature on *TiO_2* and *Ag* / water nanofluid over stretching sheet. Hamad et al. [5] studied heat transfer through non-linear stretching sheet. Yousefi [6] investigated stagnation point flow of nanofluid *TiO_2* and *Cu/H_2O* through a circular cylinder.

Benkhedda and Boufendi [7] investigated convective nanofluid flow of *Ag*/water in concentric annulus with constant heat flux on outer cylinder. Eiamsa-ard et al. [8] concluded that multiple twisted tapes and TiO_2 nanoparticle in water improves thermal performance in a heat exchanger tube. Ullah et al. [9] studied Ag-TiO_2/water hybrid nanofluid with magnetic field over cylindrical surface. Benkhedda et al. [10] numerically analysed mixed convective flow of nanofluid TiO_2 and hybrid nanofluid Ag-TiO_2 water as base fluid in an annulus. Devi et al. [11] compared heat transfer rate of nanofluid Cu/H_2O with hybrid nanofluid Cu-Al_2O_3/water. Rizk et al. [12] studied thermal heat transfer in hybrid nanofluid with the effect of heat source and magnetic field. Chahregh et al. [13] studied a mathematical model for Ag-TiO_2 hybrid nanofluid with pure blood as base fluid past the porous channel. Esfe et al. [14] compared the experimental data of thermal conductivity of *SWCNT-MgO* with *MgO* and *SWCNT* mono particle nanofluid in ethylene glycol as base fluid. Rostami et al. [15] studied hybrid nanofluid SiO_2-Al_2O_3 flow near the stagnation point through a permeable vertical plate. Waini [16] studied heat and mass transfer flow of Al_2O_3-Cu/water hybrid nanofluid over a moving surface. Suresh et al. [17] synthesized hybrid nanofluid Al_2O_3/H_2O using two step thermo chemical method. Ghachem et al. [18] analysed enhanced heat transfer in hybrid nanofluid flow through a rectangular wavy channels. Suresh et al. [19] presented convective heat transfer flow of hybrid nanofluid Al_2O_3-Cu/water over a uniformly heated tube. Madhesh et al. [20] investigated heat transfer of Cu–TiO_2 using a tube counter flow. Sunder et al. [21] estimated friction factor and convective heat transfer coefficient for *MWCNT–*Fe_3O_4/water hybrid nanofluids through a circular tube. Saha [22] investigated water based nanofluid Al_2O_3 and TiO_2 in a circular pipe with uniform heat flux. Nine et al. [23] investigated synthesis process of copper/cuprous oxide (Cu/Cu_2O) nanoparticles with size below 30nm. Ghadikolaei et al. [24] investigated stagnation point flow of hybrid nanofluid TiO_2-Cu/water toward a stretching sheet. Rashid et al. [25] studied the different shapes of *Ag* and TiO_2 hybrid nanofluid as sphere, blade and lamina with the effect of suction and injection over permeable stretching cylinder. Toghraie et al. [26] presented impact on the thermal conductivity of hybrid nanofluid ZnO-TiO_2/ ethylene glycol. Mohebbi et al. [27] studied thermal performance of $MWCNT$-Fe_3O_4/water hybrid nanofluid in a channel.

From an extensive review of existing literature, it can be stated that there has been no prior research conducted to investigate the influence of velocity and thermal slip conditions in a porous medium on the convective heat transfer of an MHD hybrid nanofluid over a permeable stretching surface. To the best of the authors' knowledge, this particular study has not been previously reported in the available literature. The governing partial differential equations PDEs are transformed into dimensionless nonlinear ordinary differential equations ODEs by using appropriate similarity transformations and solved analytically with Keller-box finite difference method. Notable effect of involved parameters such as velocity and thermal slip parameter, porosity parameter, magnetic parameter, Prandtl number, Eckert number on velocity, concentration and thermal profiles are analysed in graphical and tabular form with an excellent agreement with previous literature.

2. Flow Modelling

In this paper, we explore heat transfer analysis of steady incompressible hybrid nanofluid of silver and titanium dioxide $(Ag$-$TiO_2/H_2O)$ over a nonlinear permeable stretching sheet with slip conditions in porous medium (Figure1). Let two-dimensional Cartesian coordinate system (x, y), where x-axis is measured along the sheet and y-axis normal to it and the flow takes place at $y \geq 0$. The sheet is stretched with velocity $u_w = ax^n$ keeping the origin fixed, where a is a constant and n is non-linear stretching parameter. To study the effect of Lorentz force an uniform magnetic field B is applied along y-direction. The temperature and concentration are maintained constant, symbolized by T_w and C_w respectively at surface and far from the boundary they are symbolized by T_∞ and C_∞ respectively.

Under above suppositions the equations of continuity, momentum, energy and concentration that govern the flow are written as:

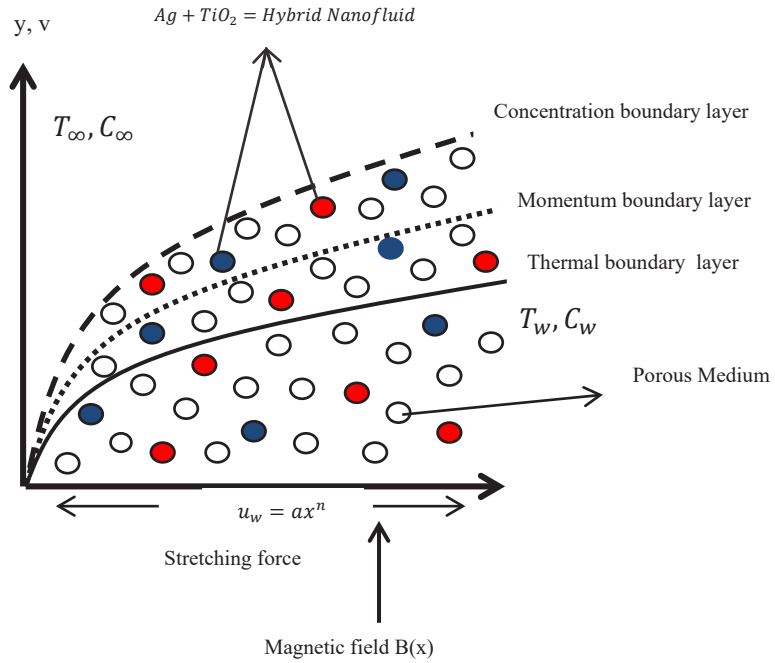

Figure 1 – Coordinate system and schematic diagram of the problem

Continuity equation

$$\frac{\partial u}{\partial x}+\frac{\partial v}{\partial y}=0\,. \tag{1}$$

Momentum equation

$$u\frac{\partial u}{\partial x}+v\frac{\partial u}{\partial y}=\nu_{hnf}\frac{\partial^2 u}{\partial y^2}-\frac{\sigma_{hnf}}{\rho_{hnf}}B^2u-\frac{\nu_{hnf}}{k'}u+$$
$$+g\left[\frac{(\rho\beta_T)_{hnf}}{\rho_{hnf}}(T-T_\infty)+\frac{(\rho\beta_C)_{hnf}}{\rho_{hnf}}(C-C_\infty)\right]. \tag{2}$$

Energy equation

$$u\frac{\partial T}{\partial x}+v\frac{\partial T}{\partial y}=\frac{k_{hnf}}{(\rho c_p)_{hnf}}\frac{\partial^2 T}{\partial y^2}+$$
$$+\frac{\mu_{hnf}}{(\rho c_p)_{hnf}}\left(\frac{\partial u}{\partial y}\right)^2+\qquad. \tag{3}$$
$$+\tau\left[\frac{D_T}{T_\infty}\left(\frac{\partial T}{\partial y}\right)^2+D_B\frac{\partial T}{\partial y}\frac{\partial C}{\partial y}\right]$$

Concentration equation

$$u\frac{\partial C}{\partial x}+v\frac{\partial C}{\partial y}=D_B\frac{\partial^2 C}{\partial y^2}+\frac{D_T}{T_\infty}\frac{\partial^2 T}{\partial y^2}\,. \tag{4}$$

The appropriate boundary conditions as per formulation are prescribed as:

$$At\ \text{y=0},\ u=u_w+N\nu_f\frac{\partial u}{\partial y},$$
$$v=v_w, T=T_w+D\frac{\partial T}{\partial y}, C=C_w \tag{5}$$
$$At\ \text{y}\to\infty,\ u=0,\quad v=0, T=T_\infty, C=C_\infty$$

Here $T_w=T_\infty+bx^{2n}$, b is a constant. Velocity slip factor $N=N_1x^{\frac{-n-1}{2}}$ which proportional to x with N_1 initial value of velocity slip. Thermal slip factor $D=D_1x^{\frac{-n-1}{2}}$ which proportional to x with D_1 initial value of thermal slip.

Similarity variables are introduced as follow:

$$\eta = y\left(\frac{a(n+1)}{2\nu_f}\right)^{\frac{1}{2}} x^{\left(\frac{n-1}{2}\right)};\ u = ax^n f'(\eta);$$

$$v = -\left(\frac{(n+1)a\nu_f}{2}\right)^{\frac{1}{2}} x^{\left(\frac{n-1}{2}\right)}\left[f(\eta)+\frac{n-1}{n+1}\eta f'(\eta)\right];$$

$$T = T_\infty + bx^{2n}\theta(\eta);\ \phi(\eta) = \frac{C-C_\infty}{C_w-C_\infty}. \qquad (6)$$

Using equation (6), equations (1)-(5) are written as:

$$f''' - \frac{\nu_f}{\nu_{hnf}}\left(\frac{2n}{n+1}f'^2 - ff''\right) - \frac{2}{n+1}\frac{\sigma_{hnf}}{\sigma_f}\frac{\mu_f}{\mu_{hnf}}Mf' - \frac{2}{n+1}f'd + \frac{2}{n+1}\frac{\nu_f}{\nu_{hnf}}\frac{(\beta_T)_{hnf}}{(\beta_T)_f}\frac{Gr_x}{\mathrm{Re}_x^2}\theta + \frac{2}{n+1}\frac{\nu_f}{\nu_{hnf}}\frac{(\beta_C)_{hnf}}{(\beta_C)_f}\frac{Gc_x}{\mathrm{Re}_x^2}\phi = 0 \qquad (7)$$

$$\frac{\theta''}{\mathrm{Pr}} + \frac{\mu_{hnf}}{\mu_f}\frac{k_f}{k_{hnf}}Ecf''^2 + \frac{k_f}{k_{hnf}}\frac{(\rho c_p)_{hnf}}{(\rho c_p)_f}\times \left[N_t\theta'^2 + N_b\theta'\phi' + f\theta' - \frac{4n}{n+1}f'\theta\right] = 0 \qquad (8)$$

$$\phi'' + Lef\phi' + \frac{N_t}{N_b}\theta'' = 0 \qquad (9)$$

$$f(0) = S, f'(0) = 1+\lambda_1 f''(0), \theta(0) = 1+\lambda_2\theta'(0), \phi(0) = 1 \text{ and}$$

$$f'(\infty) = 0, \theta(\infty) = 0, \phi(\infty) = 0 \qquad (10)$$

where $M = \frac{2\sigma_f B_0^2}{a(n+1)\rho_f}$, $S = -\frac{v_w}{\sqrt{a\nu_f}}$, $d = \frac{2\nu_f}{a(n+1)Kx^{-n-1}}$, $Gr_x = \frac{g\beta_T(T_w-T_\infty)x^3}{\nu^2}$, $Gc_x = \frac{g\beta_C(C_w-C_\infty)x^3}{\nu^2}$, $Le = \frac{\alpha}{D_B}$, $\mathrm{Pr} = \frac{\nu}{\alpha}$, $N_b = \frac{\tau D_B}{\nu_f}(C_w-C_\infty)$, $N_t = \frac{\tau D_T}{T_\infty}\frac{(T_w-T_\infty)}{\nu_f}$.

The skin-friction coefficient C_f, Nusselt number *Nu* and Sherwood number *Sh* that characterize this study are given by:

$$C_{fx} = \frac{\mu_f}{\rho_f u_w^2}\left.\frac{\partial u}{\partial y}\right|_{y=0},\ Nu_x = \frac{xq_w}{k(T_w-T_\infty)},$$

$$Sh_x = \frac{xq_m}{D_B(C_w-C_\infty)} \qquad (11)$$

where $q_w = \left.\frac{\partial T}{\partial y}\right|_{y=0}$ is heat flux and $q_m = -D_B\left.\frac{\partial C}{\partial y}\right|_{y=0}$ is mass flux at surface with thermal conductivity *k*.

Using (6) equations (11) become

$$\mathrm{Re}_x^{\frac{1}{2}} C_{fx} = \sqrt{\frac{n+1}{2}}f''(0),$$

$$\mathrm{Re}_x^{-\frac{1}{2}} Nu_x = -\sqrt{\frac{n+1}{2}}\theta'(0),$$

$$\mathrm{Re}_x^{\frac{1}{2}} Sh_x = -\sqrt{\frac{n+1}{2}}\phi'(0), \qquad (12)$$

here local Reynolds number $Re_x = \frac{u_w x}{\nu}$.

Hybrid nanofluid model

Thermophysical properties of the hybrid nanofluid of silver-titanium dioxide/water *(Ag-TiO2/H2O)* are given as:

Hybrid nanofluid dynamic viscosity

$$\frac{\mu_{hnf}}{\mu_f}=\frac{1}{\left(1-\phi_{Ag}-\phi_{TiO_2}\right)^{2.5}}.$$

Hybrid nanofluid density

$$\frac{\rho_{hnf}}{\rho_f}=\left(1-\phi_{Ag}-\phi_{TiO_2}\right)+\phi_{Ag}\frac{\rho_{Ag}}{\rho_f}+\phi_{TiO_2}\frac{\rho_{TiO_2}}{\rho_f}.$$

Hybrid nanofluid specific heat capacity

$$\frac{\left(\rho c_p\right)_{hnf}}{\left(\rho c_p\right)_f}=\left(1-\phi_{Ag}-\phi_{TiO_2}\right)+ +\phi_{Ag}\frac{\left(\rho c_p\right)_{Ag}}{\left(\rho c_p\right)_f}+\phi_{TiO_2}\frac{\left(\rho c_p\right)_{TiO_2}}{\left(\rho c_p\right)_f}.$$

Hybrid nanofluid thermal conductivity

$$\frac{k_{hnf}}{k_f}=\left[\frac{2k_f+\left(\frac{\phi_{Ag}k_{Ag}+\phi_{TiO_2}k_{TiO_2}}{\phi_{Ag}+\phi_{TiO_2}}\right)+2\left(\phi_{Ag}k_{Ag}+\phi_{TiO_2}k_{TiO_2}\right)-2\left(\phi_{Ag}+\phi_{TiO_2}\right)k_f}{2k_f+\left(\frac{\phi_{Ag}k_{Ag}+\phi_{TiO_2}k_{TiO_2}}{\phi_{Ag}+\phi_{TiO_2}}\right)-\left(\phi_{Ag}k_{Ag}+\phi_{TiO_2}k_{TiO_2}\right)+\left(\phi_{Ag}+\phi_{TiO_2}\right)k_f}\right]$$

Thermal and solutal volumetric coefficient

$$\left(\rho\beta_T\right)_{hnf}= =\left(1-\phi_{TiO_2}\right)\left(\left(\rho\beta_T\right)_{Ag}\phi_{Ag}+\left(1-\phi_{Ag}\right)\left(\rho\beta_T\right)_f\right)+ +\phi_{TiO_2}\left(\rho\beta_T\right)_{TiO_2}$$

$$\left(\rho\beta_C\right)_{hnf}= =\left(1-\phi_{TiO_2}\right)\left(\left(\rho\beta_C\right)_{Ag}\phi_{Ag}+\left(1-\phi_{Ag}\right)\left(\rho\beta_C\right)_f\right)+ +\phi_{TiO_2}\left(\rho\beta_C\right)_{TiO_2}$$

where ϕ_{Ag} and ϕ_{TiO2} specify the solid volume fraction of *Ag* and TiO_2.

Thermophysical properties of base fluid water and nanofluid are:

Physical properties	Base fluid	Nanoparticles	
	H_2O	*Ag*	TiO_2
$\sigma(1/\Omega m)$	0.05	2.6×10^6	6.30×10^7
$\rho(kgm^{-3})$	997.10	10500	4250
$Cp(Jkg^{-1}K^{-1})$	4179	235	686
$k(Wm^{-1}K^{-1})$	0.620	429	8.9538
$\beta_T\times10^5(1/K)$	21	1.89	0.9

3. Solution Methodology

Keller box finite difference method is used to solve the formulated problem. In the first step

Let $f'=r,\ f''=r'=s,\ \theta'=t,\ \phi'=w$

For, these assumptions the higher order ODEs (7)-(10) are altered to first order ODEs as follow:

$$s'-\frac{\nu_f}{\nu_{hnf}}\left(\frac{2n}{n+1}r^2-fs\right)-\frac{2M}{n+1}\frac{\sigma_{hnf}}{\sigma_f}\frac{\mu_f}{\mu_{hnf}}r- -\frac{2d}{n+1}r+\frac{2}{n+1}\frac{\nu_f}{\nu_{hnf}}\frac{(\beta_T)_{hnf}}{(\beta_T)_f}\frac{Gr_x}{\mathrm{Re}_x^2}\theta+ +\frac{2}{n+1}\frac{\nu_f}{\nu_{hnf}}\frac{(\beta_C)_{hnf}}{(\beta_C)_f}\frac{Gc_x}{\mathrm{Re}_x^2}\phi=0 \tag{13}$$

$$\frac{1}{\mathrm{Pr}}t'+\frac{\mu_{hnf}}{\mu_f}\frac{k_f}{k_{hnf}}Ec\,s^2+\frac{k_f}{k_{hnf}}\frac{\left(\rho c_p\right)_{hnf}}{\left(\rho c_p\right)_f}\times \times\left[N_t t^2+N_b tw+ft-\frac{4n}{n+1}r\theta\right]=0 \tag{14}$$

$$w'+Lefw+\frac{N_t}{N_b}t'=0 \tag{15}$$

$$f(0)=0,\ r(0)=1+\lambda_1 s(0),\\ \theta(0)=1+\lambda_2 t(0),\ \phi(0)=1 \text{ and} \\ r(\infty)=\theta(\infty)=\phi(\infty)=0 \tag{16}$$

The finite-difference form of the above equations are

$$\left.\begin{aligned}
&(f_j-f_{j-1})-\frac{h_j}{2}(r_j+r_{j-1})=0\\
&(r_j-r_{j-1})-\frac{h_j}{2}(s_j+s_{j-1})=0\\
&(\theta_j-\theta_{j-1})-\frac{h_j}{2}(t_j+t_{j-1})=0\\
&(\phi_j-\phi_{j-1})-\frac{h_j}{2}(w_j+w_{j-1})=0
\end{aligned}\right\} \tag{17}$$

For these centralized forms equations (13-16) will take the following form:

$$\begin{aligned}
&s_j-s_{j-1}-\frac{\nu_f}{\nu_{hnf}}h_j\left(\frac{2n}{n+1}r^2_{j-1}-(fs)_{j-\frac{1}{2}}\right)-\\
&-\frac{\sigma_{hnf}}{\sigma_f}\frac{\mu_f}{\mu_{hnf}}Mh_j(r)_{j-\frac{1}{2}}-\frac{2h_jd}{n+1}(r)_{j-\frac{1}{2}}+\\
&+\frac{2h_j}{n+1}\frac{\nu_f}{\nu_{hnf}}\frac{(\beta_T)_{hnf}}{(\beta_T)_f}\frac{Gr_x}{\mathrm{Re}_x^2}\theta_{j-\frac{1}{2}}+\\
&+\frac{2h_j}{n+1}\frac{\nu_f}{\nu_{hnf}}\frac{(\beta_C)_{hnf}}{(\beta_C)_f}\frac{Gc_x}{\mathrm{Re}_x^2}\phi_{j-\frac{1}{2}}=0
\end{aligned} \tag{18}$$

$$\frac{1}{\mathrm{Pr}}(t_j-t_{j-1})+\frac{\mu_{hnf}}{\mu_f}\frac{k_f}{k_{hnf}}h_jEc.s^2_{j-1}+\frac{k_f}{k_{hnf}}\frac{(\rho c_p)_{hnf}}{(\rho c_p)_f}\times \\ \times\left[N_t t^2_{j-1}+N_b(tw)_{j-\frac{1}{2}}+(ft)_{j-\frac{1}{2}}-\frac{4n}{n+1}(r\theta)_{j-\frac{1}{2}}\right]=0 \tag{19}$$

$$w_j-w_{j-1}+h_jLe(fw)_{j-\frac{1}{2}}+\frac{N_t}{N_b}(t_j-t_{j-1})=0 \tag{20}$$

$$f_0=S,\ r_0=1+\lambda_1 s(0),\ \theta_0=1+\lambda_2 t(0),\\ \phi_0=1,\ r_j=0,\ \theta_j=0,\ \phi_j=0 \tag{21}$$

Newton's Method

By means of newton's method we linearized the non-linear system using following iterates:

$$\left.\begin{aligned}
f_j^{(m+1)}&=f_j^{(m)}+\delta f_j^{(m)}\\
r_j^{(m+1)}&=r_j^{(m)}+\delta r_j^{(m)}\\
s_j^{(m+1)}&=s_j^{(m)}+\delta s_j^{(m)}\\
\theta_j^{(m+1)}&=\theta_j^{(m)}+\delta\theta_j^{(m)}\\
t_j^{(m+1)}&=t_j^{(m)}+\delta t_j^{(m)}\\
\phi_j^{(m+1)}&=\phi_j^{(m)}+\delta\phi_j^{(m)}\\
w_j^{(m+1)}&=w_j^{(m)}+\delta w_j^{(m)}
\end{aligned}\right\} \tag{22}$$

$m=0,1,2,3.....$

Substituting Equation (22) in equations (18-21) we have the following tridiagonal system.

$$\delta f_j-\delta f_{j-1}-\frac{h_j}{2}(\delta r_j+\delta r_{j-1})=(a_1)_{j-\frac{1}{2}} \tag{23}$$

$$\delta r_j-\delta r_{j-1}-\frac{h_j}{2}(\delta s_j+\delta s_{j-1})=(a_2)_{j-\frac{1}{2}} \tag{24}$$

$$\delta\theta_j-\delta\theta_{j-1}-\frac{h_j}{2}(\delta t_j+\delta t_{j-1})=(a_3)_{j-\frac{1}{2}} \tag{25}$$

$$\delta\phi_j-\delta\phi_{j-1}-\frac{h_j}{2}(\delta w_j+\delta w_{j-1})=(a_4)_{j-\frac{1}{2}} \tag{26}$$

$$(b_1)\delta s_j+(b_2)\delta s_{j-1}+(b_3)\delta f_j+(b_4)\delta f_{j-1}+\\ +(b_5)\delta r_j+(b_6)\delta r_{j-1}=(a_5)_{j-\frac{1}{2}} \tag{27}$$

$$(c_1)\delta t_j+(c_2)\delta t_{j-1}+(c_3)\delta f_j+(c_4)\delta f_{j-1}+\\ +(c_5)\delta r_j+(c_6)\delta r_{j-1}+(c_7)\delta\theta_j+\\ (c_8)\delta\theta_{j--1}+(c_9)\delta w_j+(c_{10})\delta w_{j-1}+\\ +(c_{11})\delta s_j+(c_{12})\delta s_{j-1}=(a_6)_{j-\frac{1}{2}} \tag{28}$$

$$(d_1)\delta w_j+(d_2)\delta w_{j-1}+(d_3)\delta f_j+\\ +(d_4)\delta f_{j-1}+(d_5)\delta t_j+(d_6)\delta t_{j-1}=(a_7)_{j-\frac{1}{2}} \tag{29}$$

where

$$\left.\begin{aligned}
\left(b_1\right)_j &= 1+\frac{D_2}{D_1}\frac{h_j}{2}f_{j-\frac{1}{2}} \\
\left(b_2\right)_j &= \left(b_1\right)_j - 2 \\
\left(b_3\right)_j &= \frac{D_2}{D_1}\frac{h_j}{2}s_{j-\frac{1}{2}} \\
\left(b_4\right)_j &= \left(b_3\right)_j \\
\left(b_5\right)_j &= -\frac{D_2}{D_1}\frac{2n}{n+1}h_j r_{j-\frac{1}{2}} - \frac{M}{2}\frac{D_7}{D_1}h_j - \frac{h_j}{n+1}d \\
\left(b_6\right)_j &= \left(b_5\right)_j
\end{aligned}\right\},\quad
\left.\begin{aligned}
\left(d_1\right)_j &= 1+Le\frac{h_j}{2}f_{j-\frac{1}{2}} \\
\left(d_2\right)_j &= \left(d_1\right)_j - 2 \\
\left(d_3\right)_j &= Le\frac{h_j}{2}w_{j-\frac{1}{2}} \\
\left(d_4\right)_j &= \left(d_3\right)_j \\
\left(d_5\right)_j &= \frac{N_t}{N_b} \\
\left(d_6\right)_j &= -\left(d_5\right)_j
\end{aligned}\right\}$$

$$\left.\begin{aligned}
\left(c_1\right)_j &= \frac{1}{\mathrm{Pr}}+\frac{h_j}{2}D_3D_4\left[2N_t t_{j-\frac{1}{2}} + N_b w_{j-\frac{1}{2}} + f_{j-\frac{1}{2}}\right] \\
\left(c_2\right)_j &= \left(c_1\right)_j - \frac{2}{\mathrm{Pr}} \\
\left(c_3\right)_j &= D_3D_4\frac{h_j}{2}t_{j-\frac{1}{2}} \\
\left(c_4\right)_j &= \left(c_3\right)_j \\
\left(c_5\right)_j &= -D_3D_4\frac{h_j}{2}\frac{4n}{n+1}\theta_{j-\frac{1}{2}} \\
\left(c_6\right)_j &= \left(c_5\right)_j \\
\left(c_7\right)_j &= -D_3D_4\frac{h_j}{2}\frac{4n}{n+1}r_{j-\frac{1}{2}} \\
\left(c_8\right)_j &= \left(c_7\right)_j \\
\left(c_9\right)_j &= D_3D_4\frac{h_j N_b}{2}t_{j-\frac{1}{2}} \\
\left(c_{10}\right)_j &= \left(c_9\right)_j \\
\left(c_{11}\right)_j &= D_1D_4h_j Ecs_{j-\frac{1}{2}} \\
\left(c_{12}\right)_j &= \left(c_{11}\right)_j
\end{aligned}\right\};$$

$$
\left.
\begin{aligned}
\left(a_1\right)_j &= f_{j-1} - f_j + h_j\left(r_{j-\frac{1}{2}}\right)\\
\left(a_2\right)_j &= r_{j-1} - r_j + h_j\left(s_{j-\frac{1}{2}}\right)\\
\left(a_3\right)_j &= \theta_{j-1} - \theta_j + h_j\left(t_{j-\frac{1}{2}}\right)\\
\left(a_4\right)_j &= \phi_{j-1} - \phi_j + h_j\left(w_{j-\frac{1}{2}}\right)\\
\left(a_5\right)_j &= s_{j-1} - s_j + \frac{D_2}{D_1}\frac{2n}{n+1}r^2_{j-\frac{1}{2}} - \frac{D_2}{D_1}h_j\left(fs\right)_{j-\frac{1}{2}} + \frac{MD_7}{D_1}h_j r_{j-\frac{1}{2}} + \frac{2dh_j}{\left(n+1\right)}r_{j-\frac{1}{2}}\\
\left(a_6\right)_j &= \frac{1}{\mathrm{Pr}}\left(t_{j-1}-t_j\right) - \left(-h_j\left(ft\right)_{j-\frac{1}{2}} + h_j\left(\frac{4n}{n+1}\right)\left(r\theta\right)_{j-\frac{1}{2}} - h_j N_b\left(tw\right)_{j-\frac{1}{2}} - h_j N_t t^2_{j-\frac{1}{2}} - h_j Ec.s^2_{j-\frac{1}{2}}\right)D_3D_4\\
\left(a_7\right)_j &= w_j - w_{j-1} - h_j Le\left(fw\right)_{j-\frac{1}{2}} - \frac{N_t}{N_b}\left(t_j - t_{j-1}\right)
\end{aligned}
\right\}
$$

$$\delta f_0 = \delta r_0 = \delta s_0 = \delta\theta_0 = \delta\phi_0 = \delta r_j = \delta\theta_j = \delta\phi_j = 0$$

Block-elimination method

The linearized equations (23-29) solved by block tridiagonal structure having variables or constants. The matrix-vector form of equations (23-29) is

$$A\delta = \alpha\,. \tag{30}$$

The matrices elements are defined as

$$A = \begin{bmatrix} [A_1] & [C_1] & & & & & \\ [B_2] & [A_2] & [C_2] & & & & \\ & \ddots & \ddots & \ddots & & & \\ & & & [B_{j-1}] & [A_{j-1}] & [C_{j-1}] & \\ & & & & [B_j] & [A_j] & \end{bmatrix};\ \delta = \begin{bmatrix} [\delta_1] \\ [\delta_2] \\ \vdots \\ [\delta_{j-1}] \\ [\delta_j] \end{bmatrix} \text{ and } a = \begin{bmatrix} [a_1] \\ [a_2] \\ \vdots \\ [a_{j-1}] \\ [a_j] \end{bmatrix}$$

where

$$[A_1] = \begin{bmatrix} 0 & 0 & 0 & 1 & 0 & 0 & 0 \\ \frac{-h_j}{2} & 0 & 0 & 0 & \frac{-h_j}{2} & 0 & 0 \\ 0 & \frac{-h_j}{2} & 0 & 0 & 0 & \frac{-h_j}{2} & 0 \\ 0 & 0 & \frac{-h_j}{2} & 0 & 0 & 0 & \frac{-h_j}{2} \\ (b_2)_1 & 0 & 0 & (b_3)_1 & (b_1)_1 & 0 & 0 \\ (c_{12})_1 & (c_2)_1 & (c_{10})_1 & (c_3)_1 & (c_{11})_1 & (c_1)_1 & (c_9)_1 \\ 0 & (d_6)_1 & (d_2)_1 & (d_2)_1 & 0 & (d_5)_1 & (d_1)_1 \end{bmatrix}$$

$$2 \le j \le J:$$

$$[A_j]=\begin{bmatrix} \frac{-h_j}{2} & 0 & 0 & 1 & 0 & 0 & 0 \\ -1 & 0 & 0 & 0 & \frac{-h_j}{2} & 0 & 0 \\ 0 & -1 & 0 & 0 & 0 & \frac{-h_j}{2} & 0 \\ 0 & 0 & -1 & 0 & 0 & 0 & \frac{-h_j}{2} \\ (b_6)_j & 0 & 0 & (b_3)_j & (b_1)_j & 0 & 0 \\ (c_6)_j & (c_8)_j & 0 & (c_3)_j & (c_{11})_j & (c_1)_j & (c_9)_j \\ 0 & 0 & 0 & (d_3)_j & 0 & (d_5)_j & (d_1)_j \end{bmatrix};$$

$$[B_j]=\begin{bmatrix} 0 & 0 & 0 & -1 & 0 & 0 & 0 \\ 0 & 0 & 0 & 0 & \frac{-h_j}{2} & 0 & 0 \\ 0 & 0 & 0 & 0 & 0 & \frac{-h_j}{2} & 0 \\ 0 & 0 & 0 & 0 & 0 & 0 & \frac{-h_j}{2} \\ 0 & 0 & 0 & (b_4)_j & (b_2)_j & 0 & 0 \\ 0 & 0 & 0 & (c_4)_j & (c_{12})_j & (c_2)_j & (c_{10})_j \\ 0 & 0 & 0 & (d_4)_j & 0 & (d_6)_j & (d_2)_j \end{bmatrix};$$

$$[C_j]=\begin{bmatrix} \frac{-h_j}{2} & 0 & 0 & 0 & 0 & 0 & 0 \\ 1 & 0 & 0 & 0 & 0 & 0 & 0 \\ 0 & 1 & 0 & 0 & 0 & 0 & 0 \\ 0 & 0 & 1 & 0 & 0 & 0 & 0 \\ (b_5)_j & 0 & 0 & 0 & 0 & 0 & 0 \\ (c_5)_j & (c_7)_j & 0 & 0 & 0 & 0 & 0 \\ 0 & 0 & 0 & 0 & 0 & 0 & 0 \end{bmatrix}$$

$$L=\begin{bmatrix} [\alpha_1] & & & & & & \\ [\beta_2] & [\alpha_2] & [c_2] & & & & \\ & & \ddots & & & & \\ & & & \ddots & & & \\ & & & & \ddots & & \\ & & & & & [\alpha_{j-1}] & \\ & & & & & [\beta_j] & [\alpha_j] \end{bmatrix},$$

$$[\delta_1]=\begin{bmatrix} \delta s_0 \\ \delta\theta_0 \\ \delta\phi_0 \\ \delta f_1 \\ \delta s_1 \\ \delta t_1 \\ \delta w_1 \end{bmatrix}, [\delta_j]=\begin{bmatrix} \delta s_{j-1} \\ \delta\theta_{j-1} \\ \delta\phi_{j-1} \\ \delta f_j \\ \delta s_j \\ \delta t_j \\ \delta w_j \end{bmatrix}, [a_j]=\begin{bmatrix} (r_1)_{j-\frac{1}{2}} \\ (r_2)_{j-\frac{1}{2}} \\ (r_3)_{j-\frac{1}{2}} \\ (r_4)_{j-\frac{1}{2}} \\ (r_5)_{j-\frac{1}{2}} \\ (r_6)_{j-\frac{1}{2}} \\ (r_7)_{j-\frac{1}{2}} \end{bmatrix}.$$

$$U=\begin{bmatrix} [\mathrm{I}_1] & [\Gamma_{j-1}] & & & \\ & [I_1] & & & \\ & & \ddots & & \\ & & \ddots & & \\ & & \ddots & & \\ & & & [I_{j-1}] & [\Gamma_{j-1}] \\ & & & & [I] \end{bmatrix},$$

Now let the non-singular matrix A is factorized into

$$A=LU,$$

where [I] is identity matrix, $[\alpha_i]$ and $[\Gamma_i]$ are determined as follow:

$$[\alpha_i]=[A_1]$$

$$[A_1][\Gamma_1]=[C_1]$$

$$[\alpha_i]=[A_1]-[B_j][\Gamma_{j-1}], j=2,3,\ldots,J$$

$$[\alpha_j][\Gamma_j]=[C_j], j=2,3,\ldots,J-1.$$

So we have

$$LU\delta = a, Let\ U\delta = V\ and\ we\ get\ LV = a$$

$$V = \begin{bmatrix} [V_1] \\ [V_2] \\ \vdots \\ [V_{j-1}] \\ [V_j] \end{bmatrix}$$

Where, $[\alpha_1][V_1] = [a_1]$,
$[\alpha_i][V_j] = [a_j] - [B_i][V_{j-1}], 2 \le j \le J$
$[\delta_j] = [W_j], [\delta_i] = [V_j] - [\Gamma_j][\delta_{j+1}], 2 \le j \le J$

Using uniform grid of size $\triangle\eta$ =0.006 the process is continued, until the convergence criteria is satisfied.

4. Results and discussion

To analyse the physical aspects of the considered problem, a comprehensive study have been done. The graphs for fluid velocity, temperature and concentration for the different values of physical parameters such as velocity and thermal slip parameter, Prandtl number, suction parameter, magnetic parameter, Eckert number are shown in figures (2-12). By setting parameter M=1, λ=0.1, δ=0.1, S=0.5, Ec=1, Pr=6, Nb=Nt=0.1, Le=2 the numerical results for local skin friction, Nusselt and Sherwood number are presented graphically and also in tabular form (Table 1-2) with a good agreement with published literature.

Figure 2(a)-2(c) illustrates the impact of magnetic field on velocity, temperature and concentration fields respectively. Magnetic field initiates a resistive force called Lorentz force. By upsurging the value of magnetic field parameter M, the Lorentz force increases and the thickness of boundary layer reduces, therefore velocity profile decreases with an increasing magnetic field, figure 2(a). Thermal and concentration boundary layers become thicker with enhancing Lorentz force because it is a body retarding force that transverses the motion of the fluid and heat is evolved. It is shown in figure (2(b), 2(c)) that the profiles of temperature and concentrations are enhances with increasing magnetic field.

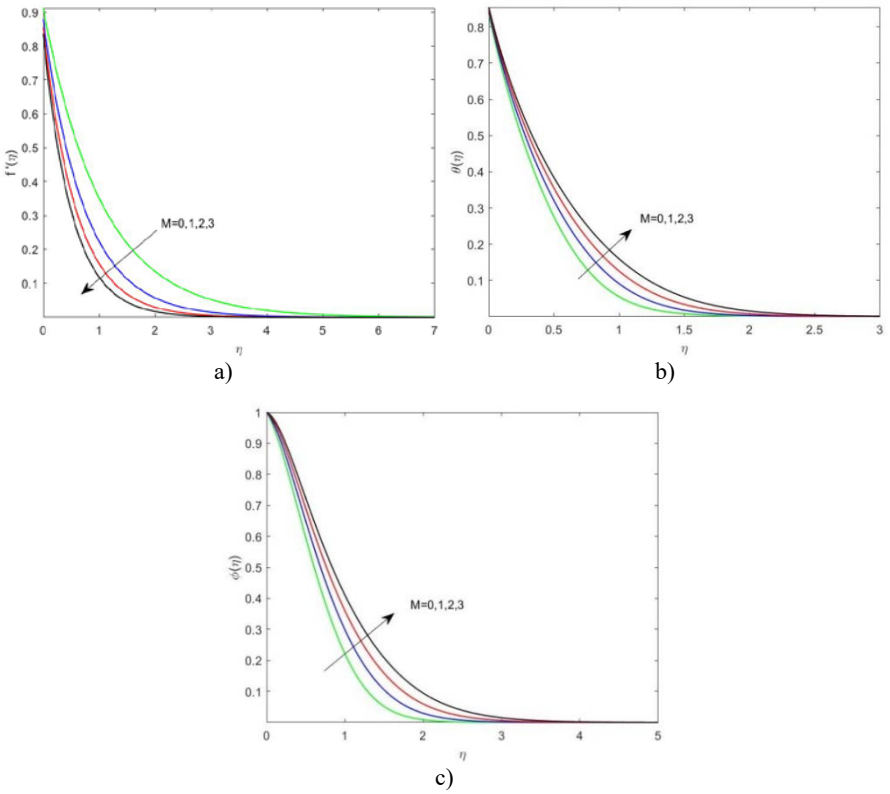

a) b) c)

Figure 2 – Effect of Magnetic parameter M on a) velocity profile, b) temperature profile, c) concentration profile

Figure 3(a)-3(c) represents the impact of the velocity slip parameter λ. As the slip condition occurs, the fluid velocity at surface is not same as the velocity of surface, therefore fluid velocity decreases as the velocity slip parameter increases, figure 3(a). Figure 3(b) and 3(c) illustrates that the temperature and concentration fields enhances with velocity slip parameter. As the thermal slip parameter δ increases, heat is transformed from the fluid to surface and the thickness of thermal boundary layer decreases.

As the thermal slip parameter δ increases, heat is mutating from the fluid to surface and the thickness of thermal boundary layer decreases. It is shown in figure 4(a) and 4(b) that the thermal and concentration profile decreases with increasing thermal slip parameter.

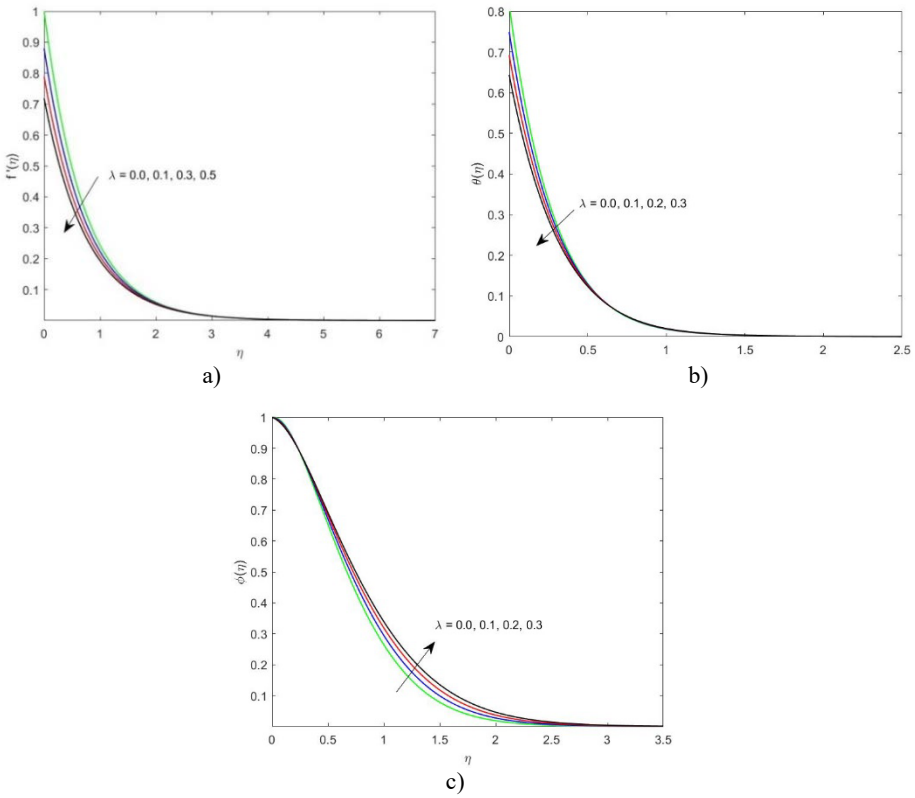

Figure 3 – Effect of velocity slip parameter λ on a) velocity profile, b) temperature profile, c) concentration profile

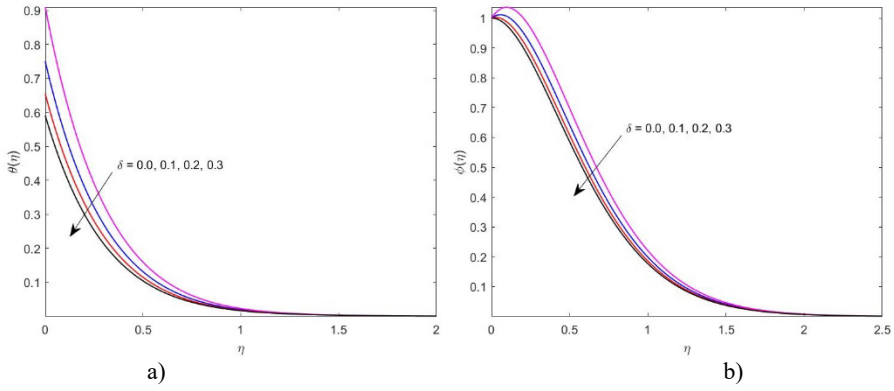

Figure 4 – Effect of thermal slip parameter δ on a) temperature profile, b) concentration profile

It is observed in figure (5) that as the suction parameter S increases, velocity profile decreases, since the suction effects retards the fluid motion. Figure (6) depicts the effects of Eckert number Ec on the thermal field θ(η). Since Eckert number (viscous dissipation parameter) is the ratio of advective heat transfer to heat dissipation potential i.e. the transformation of kinetic energy into internal energy. Due to this dissipative heat the thickness of thermal boundary layer increases and thus the temperature profile increases with increasing Eckert number Ec.

The effect of Prandtl number Pr on temperature profile is illustrates via Figure (7). Since Prandtl number is defined as the ratio between convective to conductive method of heat transfer. So heat conduction reduces due to low thermal conductivity by increasing Prandtl number. Thus the temperature profile drop off with higher Prandtl number.

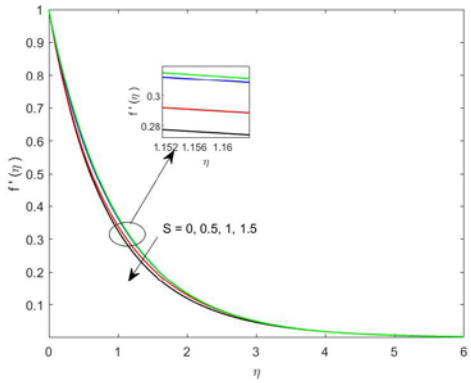

Figure 5 – Effect of suction parameter S on velocity profile

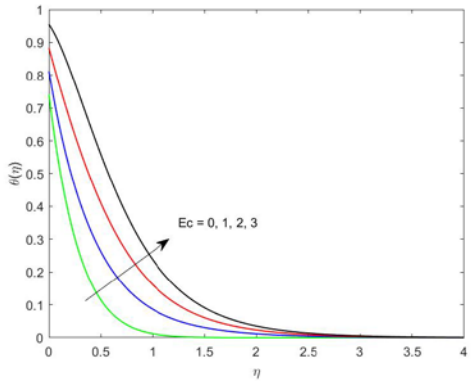

Figure 6 – Effect of Eckert number Ec on temperature profile

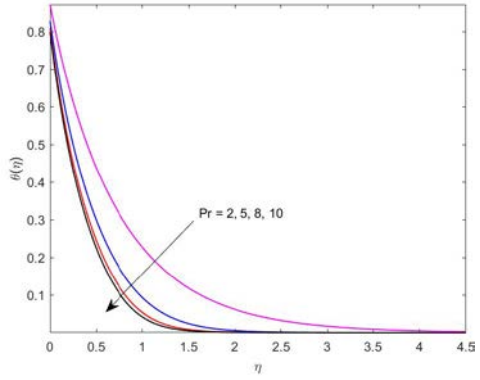

Figure 7 – Effect of Prandtl number Pr on temperature profile

Lewis number is the ratio of thermal diffusivity to species diffusivity. By enhancing the Lewis number tends to a flow separation close to the wall which results to a reduced concentration boundary layer thickness. It is observed in figure (8) that the concentration profile reduces with high Lewis number. The impacts of Brownian motion parameter Nb and thermophoresis parameter Nt are illustrate in figure 9(a)-9(c). Due to the temperature gradient, thermophoresis force and Brownian motion higher the fluid speed away from the surface and fluid is heated further. This increases the thickness of thermal boundary layer and temperature profile increases with both thermophoresis parameter Nt and Brownian motion parameter Nb, the concentration field increases with thermophoresis parameter Nt and decreases with Brownian motion parameter Nb.

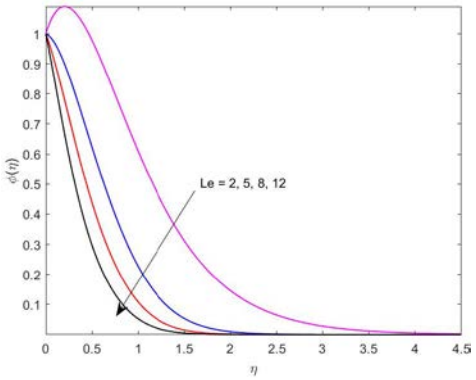

Figure 8 – Effect of Lewis number Le on concentration profile.

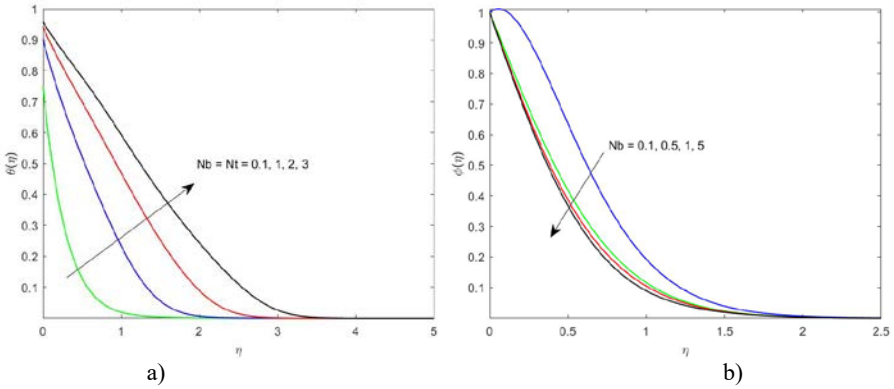

a) b)

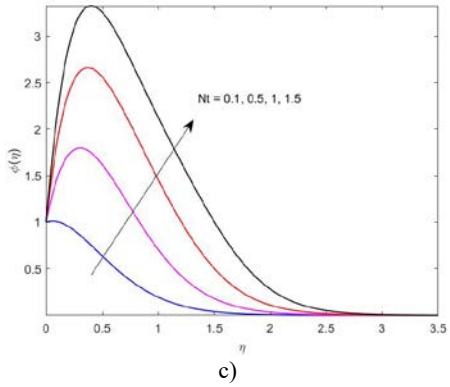

c)

Figure 9 – Effect of Brownian motion parameter Nb and thermophoresis parameter Nt on a) temperature profile, b) concentration profile, c) concentration profile

The variation in coefficient of skin-friction, Nusselt and Sherwood number for involved parameters have been depicted in figures (10-12). It is observed that the coefficient of skin-friction depreciates with both velocity slip parameter and porosity parameter. The variation in local Nusselt number for velocity and thermal slip parameters have been depicted in figures (11). It is observed that the rate of heat transfer decreases for both velocity and thermal slip, while increases for Prandtl number. Figure (12) displays the impact of Brownian motion parameter and thermophoresis number on Sherwood number, both depreciates the Sherwood number.

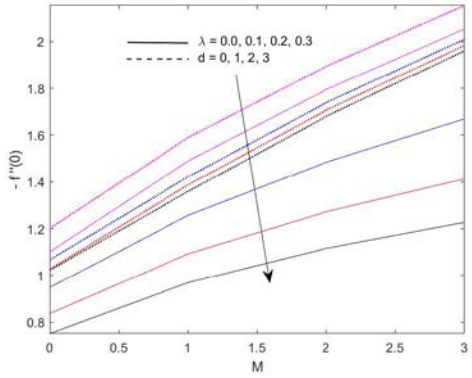

Figure 10 – Effect of velocity slip parameter λ and porosity parameter d on skin-friction coefficient

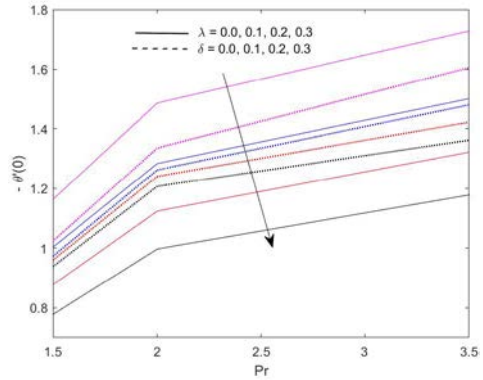

Figure 11 – Effect of velocity slip parameter λ and thermal slip parameter δ on Nusselt number

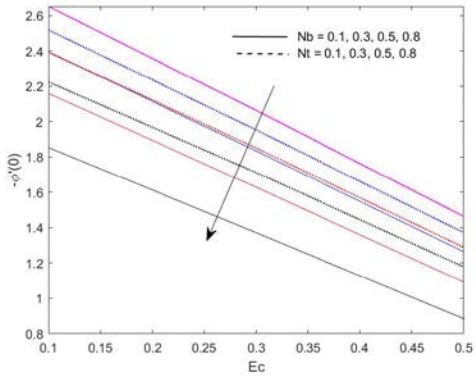

Figure 12 – Effect of Brownian motion parameter Nb and thermophoresis number Nt on Nusselt number

Table-(1) and (2) presents a comparison of the current findings with previous studies by Ramya et al.[3] and Hamad et. al.[5]. The alignment between the present results and earlier studies demonstrates a high level of consistency. Additionally, this agreement supports the reliability and accuracy of the current findings.

Table 1 – Comparison for Nusselt number and Sherwood number Pr=10, n=10, Le=10, Nt=0.3, Ec=0, M=0

Nb	$-\theta'(0)$			$\phi'(0)$		
	Ramya et al.[3]	Hamad et. al.[5]	Present Study	Ramya et al.[3]	Hamad et. al.[5]	Present Study
0.1	3.7716	3.7716	3.7715	5.6212	5.6219	5.6211
0.2	3.2514	3.2515	3.2514	0.9977	0.9981	0.9976
0.3	2.8278	2.8279	3.8277	0.4521	0.4517	0.4522

Table 2 – Comparison for skin-friction Le=1, Pr=6.8, Nb=0.1, Nt=0.1, Ec=λ=δ=M=0

n	Ramya et al. [3]	Hamad et al. [5]	Present Study
0.2	0.7675	0.7674	0.7670
0.5	0.8901	0.8901	0.8897
1.0	1.0005	1.0004	1.0003
3.0	1.1490	1.1489	1.1485
10	1.2352	1.2352	1.2346
20	1.2578	1.2577	1.2571

5. Conclusion

A computational study is done to investigate convective heat transfer on MHD hybrid nanofluid with velocity and thermal slip over a nonlinear stretching sheet in porous medium. The governing PDE's are evolved and transformed into ODE's by using suitable similarity transformations. The governing ODE's are solved by Keller-box finite difference approach by using MATLAB software. Then the following results are made:

- Velocity slip, thermal slip, and the presence of a magnetic field result in a reduction of the velocity field. While, the velocity field is enhanced by the porosity parameter and the Lewis number.
- Velocity slip, thermal slip, and a high Prandtl number lead to a decrease in the temperature field. Conversely, the temperature field is enhanced by higher Eckert number, Lewis number, the presence of a magnetic field, the Brownian motion parameter, and the thermophoresis parameter.
- The concentration field diminishes as the Brownian motion parameter, porosity parameter, thermal slip, and Lewis number increase, while it improves with higher thermophoresis parameter, magnetic field, and velocity slip.
- Skin friction coefficient improves for magnetic parameter and depreciates for velocity slip parameter and porosity parameter.
- Nusselt number improves for Prandtl number, while depreciate for velocity and thermal slip parameter.
- Sherwood number depreciates for increasing Eckert number, Brownian motion parameter and thermophoresis number.

Nomenclature:

u, v Velocity components in x and y axis, respectively (unit: $m.s^{-1}$).
u_w Stretching velocity of the sheet (unit: ms^{-1}).
n Non linear stretching parameter.
B Magnetic field strength (unit: $A.m^{-1}$).
g Gravitational acceleration ($m.s^{-2}$).
β_T Temperature convection coefficient.
β_c Concentration convection coeffient.
μ Dynamic viscosity (unit: $kg.m^{-1}.s^{-1}$).
ν Kinematic viscosity (unit: $m^2.s^{-1}$).
ρ Density of the fluid ($kg.m^{-3}$).
σ Electrical conductivity ($S.m^{-1}$).
k' Permeability of porous medium.
φ Volume fraction.
λ Velocity slip parameter.
δ Thermal slip parameter.
T Temperature.
C Concentration.
d Porosity parameter.
c_p Specific heat capacity ($J.kg^{-1}.K$)
Ag Silver.
TiO_2 Titanium Dioxide.
Le Lewis number.
M Magnetic parameter.
Nb Brownian motion parameter.
Nt Thermophoresis parameter.
N_1 Initial velocity slip.
D_1 Initial thermal slip.
Pr Prandtl number.
S Suction parameter.
Gr Thermal Grashof number.
Gc Solutal Grashof number.
Ec Eckert number.
Re Reynolds number.

Subscripts

f Base fluid water.
∞ Conditions far away from the surface.
w Conditions at the surface.
nf Nanofluid.
hnf Hybrid nanofluid.

Funding

This research has been conducted with financial assistance from UGC, India, in the form of a senior research fellowship under UGC-Ref. No.: 1294/ (CSIR-UGC NET JUNE 2019), granted to Suman Sharma.

References

1. Abu-Nada, E. “Effects of Variable Viscosity and Thermal Conductivity of CuO-Water Nanofluid on Heat Transfer Enhancement in Natural Convection: Mathematical Model,” *J. Heat Transfer*. May 2010, 132(5): 052401, doi: 10.1115/1.4000440.

2. Hejazian, M., Moraveji, M.K. "A comparative analysis of single and two-phase models of turbulent convective heat transfer in a tube for TiO2 nanofluid with CFD." *Numerical Heat Transfer, Part A: Applications* 63, 10 (2013): 795-806, doi: 10.1080/10407782.2013.756759.

3. Ramya, D., Raju, R.S., Rao, J.A., Chamkha, A.J. “Effects of velocity and thermal wall slip on magnetohydrodynamics (MHD) boundary layer viscous flow and heat transfer of a nanofluid over a non-linearly-stretching sheet: a numerical study,” *Propuls. Power Res.* 7, 2 (2018): 182-95., doi: 10.1016/j.jppr.2018.04.003.

4. Acharya, N., Das, K., Kundu, P. K. “Ramification of variable thickness on MHD TiO 2 and Ag nanofluid flow over a slendering stretching sheet using NDM.” *The European physical journal plus* 131 (2016): 1-16., doi: 10.1140/epjp/i2016-16303-4.

5. Hamad, M. A. A. “Analytical solution of natural convection flow of a nanofluid over a linearly stretching sheet in the presence of magnetic field,” *Int. Commun. Heat Mass Transf.* 38, 4 (2011): 487-92., doi: 10.1016/j.icheatmasstransfer.2010.12.042.

6. Yousefi, M., Dinarvand, S., Eftekhari Yazdi, M., Pop, I. “Stagnation-point flow of an aqueous titania-copper hybrid nanofluid toward a wavy cylinder,” *Int. J. Numer. Methods Heat Fluid Flow* 28, 7 (2018): 1716-35, doi: 10.1108/HFF-01-2018-0009.

7. Benkhedda, M., Boufendi, T. 2016. "Computational study of the mixed convection heat transfer of Ag-water nanofluid in an annular duct." In *2016 International Renewable and Sustainable Energy Conference (IRSEC)*, Marrakech, Morocco, Nov. 14-17. IEEE.

8. Eiamsa-ard, S. Kiatkittipong, K. “Heat Transfer Enhancement by Multiple Twisted Tape Inserts and TiO2/Water Nanofluid,” *Appl. Therm. Eng.* 70.1 (2014): 896-924., doi: 10.1016/j.applthermaleng.2014.05.062.

9. Ullah, A., Fatima, N., Alharbi, K.A.M., Elattar, S. “A Numerical Analysis of the Hybrid Nanofluid (Ag + TiO 2 + Water) Flow in the Presence of Heat and Radiation Fluxes.” *Energies* 16, 3 (2023): 1220.

10.Benkhedda, M., Boufendi, T., Touahri, S. "Laminar mixed convective heat transfer enhancement by using Ag-TiO 2-water hybrid Nanofluid in a heated horizontal annulus." *Heat and Mass Transfer* 54 (2018): 2799-814. doi: 10.1007/s00231-018-2302-x.

11.Devi, S. P. A., Devi, S. S. U. "Numerical investigation of hydromagnetic hybrid Cu–Al2O3/water nanofluid flow over a permeable stretching sheet with suction." *International Journal of Nonlinear Sciences and Numerical Simulation* 17, 5 (2016): 249-257.

12.Rizk, D., Ullah, A., Elattar S., Alharbi, K.A.M. “Impact of the KKL Correlation Model on the Activation of Thermal Energy for the Hybrid Nanofluid (GO + ZnO + Water) Flow through Permeable Vertically Rotating Surface,” *Energies* 15, 8 (2022): 2872.

13.Chahregh, H.S., Dinarvand, S. “TiO_2 -Ag / blood hybrid nano fl uid fl ow through an artery with applications of drug delivery and blood circulation in the respiratory system,” *International Journal of Numerical Methods for Heat & Fluid Flow* 30, 11 (2020): 4775-96., doi: 10.1108/HFF-10-2019-0732.

14.Esfe, M.H., Rostamian, S.H., Alirezaie, A. “An applicable study on the thermal conductivity of SWCNT-MgO hybrid nanofluid and price-performance analysis for energy management,” *Applied Thermal Engineering* 111 (2017): 1202-10 , doi: 10.1016/j.applthermaleng.2016.09.091.

15.Rostami, M.N., Dinarvand, S., Pop, I."Dual solutions for mixed convective stagnation-point flow of an aqueous silica–alumina hybrid nanofluid." *Chinese journal of physics* 56, 5 (2018): 2465-78., doi: 10.1016/j.cjph.2018.06.013.

16.Waini, I., Ishak, A., Pop, I. “Flow and heat transfer of a hybrid nanofluid past a permeable moving surface,” *Chinese J. Phys.* 66 (2020): 606-19, doi: 10.1016/j.cjph.2020.04.024.

17.Suresh, S., Venkitaraj, K. P., Selvakumar, P., Chandrasekar, M. “Effect of Al_2O_3 – Cu / water hybrid nanofluid in heat transfer,” *Exp. Therm. Fluid Sci.* 38 (2012): 54-60, doi: 10.1016/j.expthermflusci.2011.11.007.

18.Ghachem, K., Aich, W., Kolsi, L. “Computational analysis of hybrid nanofluid enhanced heat transfer in cross flow micro heat exchanger with rectangular wavy channels.” *Case Stud. Therm. Eng.*, 24 (2021): 100822, doi: 10.1016/j.csite.2020.100822.

19.Suresh, S., Venkitaraj, K.P., Selvakumar, P., Chandrasekar, M. "Synthesis of Al_2O_3–Cu/water hybrid nanofluids using two step method and its thermo physical properties." *Colloids and Surfaces A: Physicochemical and Engineering Aspects* 388, 1-3 (2011): 41-8. doi: 10.1016/j.colsurfa.2011.08.005.

20.Madhesh, D., Parameshwaran, R., Kalaiselvam, S. “Experimental investigation on convective heat transfer and rheological characteristics of Cu – TiO_2 hybrid nanofluids,” *Exp. Therm. Fluid Sci. 52 (2014): 104-15.* , doi: 10.1016/j.expthermflusci.2013.08.026.

21.Sundar, L.S., Singh, M.K., Sousa, A.C.M. “Enhanced heat transfer and friction factor of MWCNT–Fe_3O_4/water hybrid nanofluids.” *Int. Commun. Heat Mass Transf.* 52 (2014): 73-83, doi: 10.1016/j.icheatmasstransfer.2014.01.012.

22.Saha, G., Paul, M.C. "Numerical analysis of the heat transfer behaviour of water based Al_2O_3 and TiO_2 nanofluids in a circular pipe under the turbulent flow condition." *International Communications in Heat and Mass Transfer* 56 (2014): 96-108, doi: 10.1016/j.icheatmasstransfer.2014.06.008.

23.Nine, J., Munkhbayar, B., Rahman, M.S., Chung, H., Jeong, H. “Highly productive synthesis process of well dispersed Cu 2 O and Cu / Cu 2 O nanoparticles and its thermal characterization,” *Mater. Chem. Phys.*, 141, 2-3 (2013): 636-642., doi: 10.1016/j.matchemphys.2013.05.032.

24.Ghadikolaei, S.S., Yassari, M., Sadeghi, H., Hosseinzadeh, K., Ganji, D.D. “Investigation on thermophysical properties of Tio2-Cu/H2O hybrid nanofluid transport dependent on shape factor in MHD stagnation point flow,” *Powder Technol.* 322 (2017): 428-38. doi: 10.1016/j.powtec.2017.09.006.

25.Rashid, U., Liang, H.,. Ahmad, H, Abbas, M., Iqbal, A., Hamed, S. "Study of (Ag and TiO_2)/water nanoparticles shape effect on heat transfer and hybrid nanofluid flow toward stretching shrinking horizontal cylinder." *Results in Physics* 21 (2021): 103812. doi: 10.1016/j.rinp.2020.103812.

26.Toghraie, D., Chaharsoghi, V. A., Afrand, M. "Measurement of thermal conductivity of ZnO–TiO 2/EG hybrid nanofluid: effects of temperature and nanoparticles concentration." *Journal of Thermal Analysis and Calorimetry* 125 (2016): 527-35, doi: 10.1007/s10973-016-5436-4.

27.Mohebbi, R., Izadi, M., Amiri Delouei, A., Hasan, S. "Effect of MWCNT–Fe 3 O 4/water hybrid nanofluid on the thermal performance of ribbed channel with apart sections of heating and cooling." *Journal of Thermal Analysis and Calorimetry* 135 (2019): 3029-3042, doi: 10.1007/s10973-018-7483-5.

Information about authors:

Suman Sharma – candidate of science, PhD, Department of Mathematics, University of Rajasthan, Jaipur-302004, India., email: s9549170542@gmail.com

Shalini Jain – Doctor of science, PhD, Associate Professor, Department of Mathematics, University of Rajasthan, Jaipur-302004, India, email: drshalinijainshah@gmail.com